Simultaneous Adsorption of SO_2–NO_x from Flue Gases in a Riser Configuration

Asit K. Das, Juray De Wilde, Geraldine J. Heynderickx, and Guy B. Marin
Laboratorium voor Petrochemische Techniek, Universiteit Gent, Krijgslaan 281, S5, B-9000 Gent, Belgium

Steen B. Iversen and Karsten Felsvang
FLS miljø a/s, Ramsingsvej 30, DK-2500 Valby, Copenhagen, Denmark

Simultaneous adsorption of $SO_2 - NO_x$ is a new, promising process in treating industrial flue gases in a short-contact-time dilute phase riser with $Na/\gamma\text{-}Al_2O_3$ sorbent particles of 50 − 100 μm diameter at 370 − 430 K. A major part of the sorbent is recycled for maximum utilization of the sorbent capacity before regeneration. A steady-state model for the riser adsorber is developed by combining independently determined rate equations with a 1-D, two-phase hydrodynamic model of the riser. The simulation was validated with the operating data from a pilot-scale installation of 4.2 Nm^3/s flue-gas capacity and solid fluxes between 1 and 3 $kg \cdot m^{-2} \cdot s^{-1}$. The riser operates in an extremely dilute phase with a solid volume fraction below 7.0×10^{-4} and a slip velocity that is constant for almost the entire riser length, indicating fully developed flow. The experimental observation that an increase in the $SO_2 - NO$ ratio in the feed gas leads to a higher NO removal efficiency is explained as resulting from an increased concentration of the adsorbed SO_2. The SO_2 removal efficiency, however, may drop if free adsorption sites are not sufficiently available. Recycling of the sorbent has only a marginal effect on the NO removal, but helps to maximize the SO_2 adsorption. For the first time, the simultaneous removal of SO_2 above 95% and of NO_x above 80% is reported using a dry, regenerable sorbent in a riser reactor.

Introduction

Two of the most toxic air pollutants, SO_2 and NO_x (NO and NO_2), are emitted to the atmosphere mainly through automobile exhaust gases and industrial flue gases. The potential sources for the industrial flue gases are oil/coal-fired furnaces and boilers, gas turbines, and chemical processes involving the combustion of fuel, for example, refinery fluid catalytic cracking (FCC) units and power plants. It is absolutely necessary to effect the efficient removal and safe disposal of these pollutants in order to meet the increasingly stringent global regulations for a cleaner environment.

The currently available technologies for the treatment of industrial flue gases are multistep, that is, the removal of SO_2 and NO_x requires two separate processes. For example, the SNOX process of Haldor Topsoe (Hydrocarbon Processing, 1998), combines the wet-gas sulfuric-acid (WSA) process for SO_2 removal, and the selective catalytic reduction (SCR) process for the removal of NO_x. Another technology for SO_2 removal is a semidry process consisting of spray-dryer absorber in a circulating fluidized bed using lime as the reagent (Graf, 1985). Kiel et al. (1992) outlined the CONICO process of simultaneous removal of SO_2 and NO_x in the presence of ammonia at 573−723 K in a gas−solid trickle-flow reactor using porous silica supported CuO as the sorbent. These processes include the difficult tasks of byproduct disposal or of handling toxic gases such as ammonia. Jeh et al. (1992) described a simultaneous SO_2−NO_x removal process called NOXSO that uses a solid adsorbent in a dense fluidized bed; however, the mass transfer between the sorbent and gas phases is inefficient due to the bubbles.

The SO_2−NO_x adsorption process SNAP is a new development in the field for the simultaneous removal of SO_2 and NO_x from flue gases (Felsvang et al., 1999). It consists of two

Correspondence concerning this article should be addressed to G. B. Marin.

major steps: (1) simultaneous adsorption of SO_2-NO_x over $Na/\gamma-Al_2O_3$ sorbent, and (2) regeneration of the sorbent and further treatment of the pollutants. The adsorption step is carried out in a gas suspension adsorber (GSA), which is a very dilute phase riser. In the GSA, the raw flue gas is injected at the bottom of the riser with a combination of both recycle and regenerated sorbent particles of 50–100 microns. The flue gas pneumatically conveys the sorbent particles along the riser, and has a typical solid residence time of 5 s per pass and a temperature range of 373–423 K. The sorbent is based on $\gamma-Al_2O_3$ impregnated with Na. Fine sorbent powders entrained in the flue gas from the outlet of GSA cyclones are passed through bag filters for the control of particulates. Clean flue gas is vented to the atmosphere via a stack.

In SNAP, the regeneration of the sorbent is done in two stages. In the first stage, the spent sorbent is heated to 673 K using a heat-transfer salt in a fluidized bed with minimum air velocity. Subsequently, the sorbent is further heated in a trim heater to the regeneration temperature of 773 K. At this stage, all the NO_x adsorbed on the sorbent is released. The NO_x in this air stream is reduced to N_2 and O_2 by staged combustion with natural gas and air in the NO_x destruction burner. The NO_x-free sorbent is then treated in two fluidized beds, one with natural gas and the other with steam. In the first bed, the chemisorbed SO_2 on the sorbent reacts with methane, releasing mainly H_2S, CO_2, and a small amount of SO_2. Some sodium sulfide formed in this bed is subsequently hydrolyzed with steam, releasing additional H_2S. The combined gas from these two beds is routed to a Claus plant for recovery of elemental sulfur. The regenerated sorbent is cooled and circulated back to the GSA riser for further adsorption.

In the development of SNAP, as in most new processes, extensive studies were carried out at different stages. For example, a continuous pilot plant for the simultaneous adsorption in GSA was operated at FLS miljø, Denmark, with a flue gas capacity of 4.2 Nm^3/s. This pilot plant was used to generate process data with different operating variables, for example, riser temperature, flow rates of the flue gas and the sorbent, and inlet SO_2-NO ratio in the feed gas. The preceding data demonstrated high removal efficiencies for both SO_2 and NO_x, and a complex interaction among process variables in the GSA. In parallel, the intrinsic kinetics of the simultaneous adsorption were studied at the Laboratorium voor Petrochemische Techniek (LPT), Ghent University (RUG), Belgium, with transient step-response experiments using a fixed-bed microreactor (De Wilde and Marin, 2000). Based on these experimental data, a kinetic model was recently developed (De Wilde et al., 2000) that provides rate equations for the reactions involved in the simultaneous adsorption of SO_2 and NO_x.

The use of riser reactors is not new in the process industry. For the GSA riser, however, a major difference is that it operates in an extremely dilute phase with a solid-volume fraction typically below 10^{-3}. Also, a major part of the used sorbent is recycled externally to the bottom of the riser before its regeneration. Various models have been proposed in the literature to describe the riser hydrodynamics. The models of Wong et al. (1992) and Pugsley et al. (1992) are based on the core–annulus flow structure with semiempirical equations for calculating the length of the acceleration zone and the axial voidage profile. However, these equations are valid for a riser with moderate to high solid mass flux (60–800 kg/m^2s), whereas in the present application, the mass flux typically amounts to 2 kg/m^2s. The model of Godfroy et al. (1999) provides empirical equations to calculate the axial and radial voidage profiles in relatively dense risers with FCC catalyst and sand particles. Fei et al. (1997), while simulating FCC risers and downers, use the one-dimensional hydrodynamic model of Wong et al. (1992) with a dispersion model for both gas and solid phases. Nieuwland et al. (1997) proposed a one-dimensional hydrodynamic model based on the two-fluid approach for both the gas and solid phases. The latter model provides a sound mathematical basis for simulation of the axial-riser profiles over a wide range of operating conditions and particle characteristics. On the modeling of circulating fluidized bed (CFB) with reactions, Lin and Bleek (1990) predicts the SO_x-NO_x emissions in a CFB for coal combustion using a correlation to calculate the solid fraction profile. More advanced riser hydrodynamic models (Pita and Sundaresan, 1993; Nieuwland et al., 1996) and kinetic models (Theologos and Markatos, 1993) are also proposed. The latter models, however, require extensive computational time to converge, especially for a reactor with recycle.

In this work, a one-dimensional ideal plug-flow steady-state model for the GSA riser, obtained by combining the two fluid Eulerian-Eulerian-approach as used by Nieuwland et al. (1996) with the reaction kinetic model of De Wilde et al. (2000), is used. It consists of the mass and the momentum balance equations for the solid and gas phases. Solution of the momentum balance equations is necessary to simulate the inlet acceleration zone specially for the conical bottom riser. In addition, separate continuity equations for gas-phase components and surface species are considered. Furthermore, a simple model (without momentum balances) applicable for a fully developed flow is also used for calculating the void fraction and is compared with the results of the two-fluid model. A comparison of the simulation results with the operating data from the GSA riser pilot plant is performed. The effects of the different operating parameters are studied with the model, providing insight to the simultaneous adsorption process.

GSA Riser Operation

Pilot plant

Figure 1 shows the GSA riser pilot plant. The riser is a 15-m-long vertical pipe with a diameter of 1.6 m. The raw flue gas enters the riser at the bottom, through a bend and a diffuser. The diffuser consists of guiding plates that are placed in the bend in order to minimize the pressure drop across the bend. The regenerated sorbent and the recycle sorbent enter at the bottom of the conical section through different cyclone diplegs. The sorbent mixture is accelerated by the upward moving flue gas.

At the riser top, two cyclones separate the sorbent particles from the flue gas. The latter is passed through a bag filter for separating the sorbent fines to be sent for regeneration. The sorbent from cyclone 1 is recycled directly to the riser bottom via one L-valve with a level control (LC1). The sorbent from cyclone 2 is divided into two streams. One part is recycled back to the riser via another L-valve with a level control (LC2). The second part passes through a third L-valve,

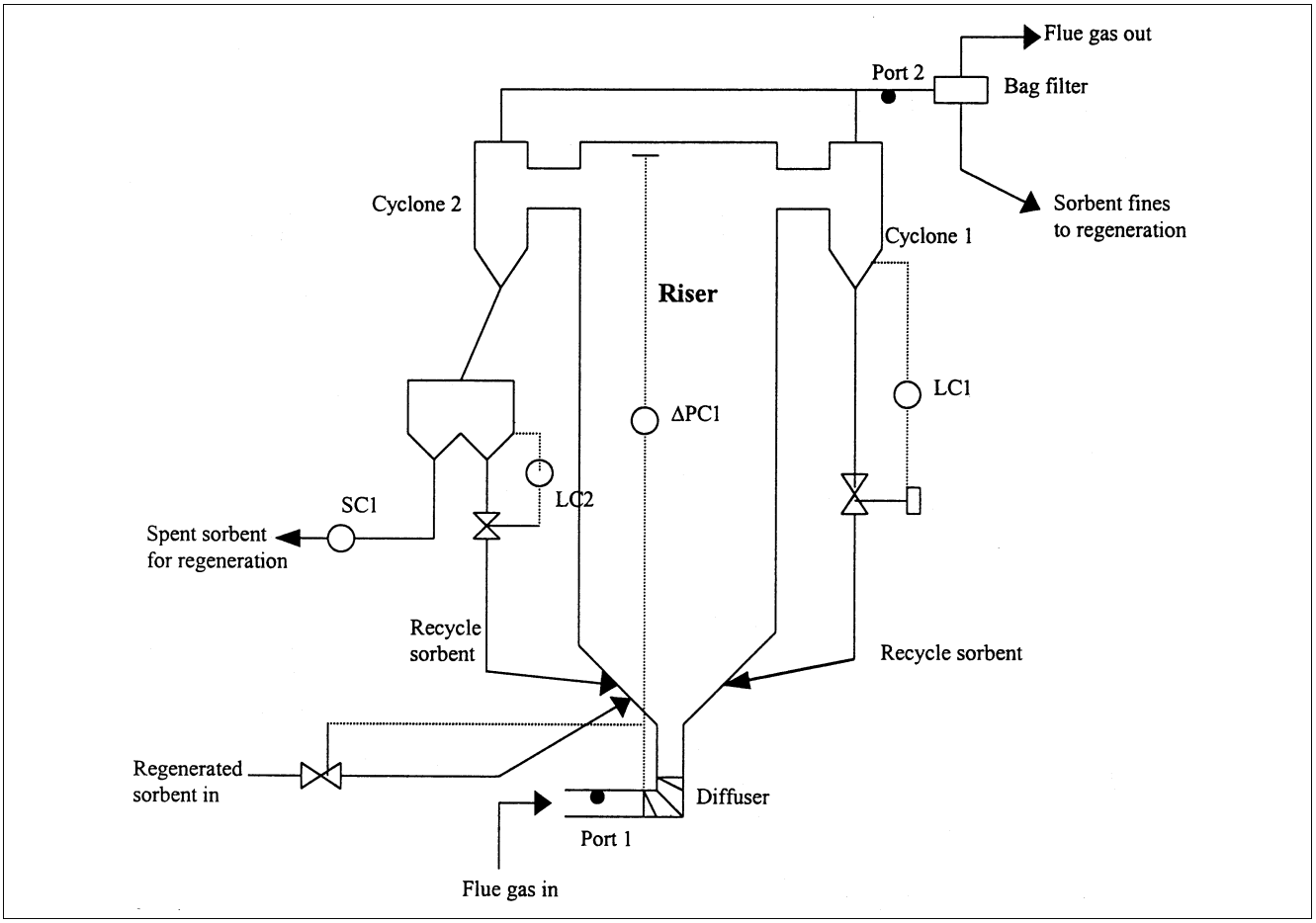

Figure 1. The GSA riser pilot plant.

but with a flow rate rather than a level control (SC1), and is directed to the sorbent regeneration unit. The set point of the flow-rate control is determined by the amount of SO_2 entering to the riser along with the flue gas.

Sorbent flow control

As shown in Figure 1, the set point of the flow rate of the regenerated sorbent to the riser is controlled by ΔPC1, which maintains a set pressure drop across the riser (bottom−top). In a normal GSA operation, the set point for SC1 is usually kept constant at an average value. In such conditions, an increase in the set point of ΔPC1 results in an increase in the flow rate of incoming regenerated sorbent and the recycled sorbent, and thus the total sorbent inside the riser. At any time, for a specified sorbent, the riser pressure drop mainly depends on the total sorbent rate and the flue gas rate inside the riser. Based on some operating data from the GSA riser with known values of riser pressure drop and sorbent/flue gas flow rates, a proprietary correlation between the riser pressure drop and these two variables has been established. Furthermore, this correlation is used to estimate the total sorbent rate from the known values of riser pressure drop and flue-gas rates. For a fixed set point of SC1 around an average value of 1 $kg \cdot s^{-1}$, the recycle sorbent flow rate is found to be three times the regenerated sorbent flow rate. This has been experimentally verified in the pilot plant from the residence time distribution of both the solid and gas phases using tracers.

Data acquisition

The concentrations of SO_2, NO, and NO_2 were measured continuously at the inlet (port 1, upstream of bend) and the outlet (port 2, between cyclone 1 and the bag filter). Additional continuous measurements of CO_2 and CO concentrations were also performed at the GSA inlet.

The analytical system at the GSA inlet is a conventional extractive system from Hartmann-Braun. The analyzers used for the measurement of SO_2 and NO_x are both of the ultraviolet type, while CO_2 and CO are measured by infrared analyzers. The concentration of NO_2 at the inlet is usually <10 ppm. Considerably higher NO_2 concentrations could potentially exist at the GSA outlet due to the SNAP adsorption chemistry. Hence, the gas analysis at the GSA outlet is designed to measure the NO_2 concentration accurately. The gas is sampled through a heated probe equipped with double filters and periodic backflushing, after which the gas is passed through a heated sample line to a selective permeation dryer (Permapure). This dryer is capable of selectively removing the

water from the gas. The gas is then passed to the analyzers. A UV analyzer from Monitor Lab is used for SO_2 analysis, and a chemiluminescence analyzer from Thermoelectron is used for the NO/NO_2 measurements.

Other important parameters monitored on a continuous basis are: flue-gas rate at the inlet, gas temperatures and pressures at both inlet and outlet, and the pressure in the conical bottom part and at the extreme top of the riser. The temperature of the regenerated sorbent at the riser inlet is about 30 K higher than that of the gas-phase temperature. However, due to the excellent radial mixing at the conical section of the riser bottom, a homogeneous temperature is attained almost instantaneously between the sorbent and the gas phases.

Data selection

The GSA pilot plant is equipped with an automatic data-acquisition system for monitoring the operation on a continuous basis. A large amount of data has been generated for a period of about two years, covering different types of sorbents and operating conditions. From the preceding data bank, initially about 4000 data points were randomly selected for the model validation. Each data point is presumed to correspond to a steady state and is collected after a time interval of at least 2 min, and frequently 30 min. So, in a way, each data point can be considered as independent in the continuous array of data. However, in the selected data set, there are some periods involving startup and fluctuations. Also, there are a lot of data (about 3000 points) where all process parameters were almost the same. The latter points are therefore not included in the model validation. To summarize, about 1000 data points were finally selected for the modeling study, which include two types of sorbents and the effect of important variables such as sorbent flow rates and an inlet SO_2/NO ratio. Typical operating ranges for major variables in the final data set, are summarized in Table 1.

Sorbent

The two sorbents are mainly used in the pilot-plant study. Sorbent A is fresh, and Sorbent B is equilibrated after passing through several adsorption–regeneration cycles in the SNAP pilot plant. The relevant properties of Sorbent A, which was also used in the kinetic studies, have been summarized previously (De Wilde et al., 2000).

Table 1. Experimental Conditions in the Pilot Plant for the Simultaneous Adsorption of SO_2–NO_x

Parameter		Range
Flue-gas rate	kmol/s	0.11–0.22
Regenerated sorbent rate	kg/s	0.42–1.52
Flue-gas outlet temperature	K	400–430
SO_2 at inlet	ppm	0–2,000
NO at inlet	ppm	0–1,000
O_2 at inlet	ppm	20,000
NO_2 at inlet	ppm	10

Reactor Model Development

Model assumptions

Isothermal, steady-state GSA operation is assumed. Both the gas and the solid phases are assumed to be plug flow. Axial gas backmixing is negligible for a bed with very low suspension density, as in the case of a GSA riser (Brereton et al., 1988). The radial variations of flow fields are also neglected for the GSA riser, due to the turbulent velocity fields associated with a high gas-phase Reynolds number ($Re \approx 10^5$) and small thickness of the annulus at very low mass flux, < 2 kg m^{-2} s^{-1} (Patience and Chaouki, 1993). In fact a 3-D simulation of the GSA riser shows uniform solid fraction for most of the riser cross section. The viscous forces are not included in the momentum balance since in the riser flow convective transport dominates in the axial direction (Nieuwland et al., 1997). Source terms related to the adsorption are neglected in the momentum balances of the gas and solid phases.

Model equations

The continuity equations for different gas-phase components and surface species are given by Eqs. 1 and 2. Here, C_i is the concentration of component i in the gas phase (mol·m_{gas}^{-3}) and θ_j is the fractional coverage by the species j of the sorbent ($mol_{species} \cdot mol_{site}^{-1}$).The net production rates R_i and R_j of various components and species are taken from the kinetic model described by De Wilde et al. (2000), with certain modifications as explained later. Overall continuity equations for gas and solid phases are given by Eqs. 3 and 4.

One-Dimensional Hydrodynamic Model. In this model, the momentum equations for gas and solid phases are given by Eqs. 5 and 6. It can be noted that for the conical bottom section, the cross-sectional surface area A is a function of riser height z. Hence, A appears inside the differential operators in all these equations. However, in Eqs. 5 and 6, A is kept outside of the dP/dz term, to take care of the side wall normal force of the gas-phase pressure due to the change in the cross-sectional surface area (Gidaspow, 1994).

The constitutive equations for the volumetric gas- and solid-phase wall frictional forces $F_{w,g}$ and $F_{w,s}$, the interphase momentum transfer coefficient β, and the drag coefficient C_D are obtained from Nieuwland et al. (1997).

$$\frac{d}{dz}\left(\epsilon_g u_g C_i A\right) = A\left(1-\epsilon_g\right)\rho_s C_t R_i \tag{1}$$

$$\frac{d}{dz}\left[\left(1-\epsilon_g\right)\rho_s u_s A \theta_j\right] = A\left(1-\epsilon_g\right)\rho_s R_j \tag{2}$$

$$\frac{d}{dz}\left(\epsilon_g \rho_g u_g A\right) = A\left(1-\epsilon_g\right)\rho_s C_t \sum_i R_i M_i \tag{3}$$

$$\frac{d}{dz}\left(\left(1-\epsilon_g\right)\rho_s u_s A\right) = -A\left(1-\epsilon_g\right)\rho_s C_t \sum_i R_i M_i \tag{4}$$

$$\frac{d}{dz}\left(\epsilon_g \rho_g u_g^2 A\right) = -\epsilon_g A\frac{dP}{dz} - \beta A(u_g - u_s) - A\epsilon_g \rho_g g + AF_{w,g} \tag{5}$$

$$\frac{d}{dz}\left[\left(1-\epsilon_g\right)\rho_s u_s^2 A\right] = -\left(1-\epsilon_g\right)A\frac{dP}{dz} + \beta A(u_g - u_s) - A\left(1-\epsilon_g\right)\rho_s g + AF_{w,s}. \tag{6}$$

Inlet Boundary Conditions. The inlet conditions for Eq. 1 are:

$$C_i = C_{io}, \tag{7}$$

where C_{io} is the concentration of the gas-phase component i at the inlet. For Eq. 2, the inlet conditions are:

$$\theta_j = \theta_{jmo} = \left(G_{so,rg}\theta_{jo,rg} + G_{so,rc}\theta_{jo,rc}\right)/\left(G_{so,rg} + G_{so,rc}\right), \tag{8}$$

where θ_{jmo} is the coverage of species j for the combined (recycle + regenerated) sorbent at the inlet. $G_{so,rg}$ and $G_{so,rc}$ are the flow rates of the regenerated and the recycle sorbents at the riser inlet. Usually, for a fully regenerated sorbent $\theta_{jo,rg}$ are considered as zero. However, for the recycle sorbent, the species coverages $\theta_{jo,rc}$ are obtained iteratively, starting with initial guesses for $\theta_{jo,rc}$ in the first iteration and the calculated values of $\theta_{j,rc}$ at the riser outlet for the subsequent iterations.

The gas and solid flow rates F_g and G_s are expressed in terms of primary variables as follows:

$$F_g = \epsilon_g u_g \rho_g A \tag{9}$$

$$G_s = G_{s,rg} + G_{s,rc} = \left(1-\epsilon_g\right)\rho_s u_s A. \tag{10}$$

For Eq. 3, the gas flow rate F_g at the inlet is provided. However, for Eq. 4, the flow rates at the inlet, $G_{so,rg}$ and $G_{so,rc}$, are obtained from a correlation based on the riser pressure drop, as discussed in the second section, leading to an inlet value of G_s.

The inlet pressure from which the density of the gas is calculated is supplied to the model using ideal gas law. In addition, an inlet value of the void fraction ϵ_g is estimated from the equation given by Rhodes (1998), which corresponds to the void fraction at the safe transport velocity, typically two times the choking velocity. The latter is calculated from the correlation given by Bi and Fan (1991) for Geldert-A particles, and implies the transition between the dense phase conveying and pneumatic transport regimes. The gas and solid velocities u_g and u_s are then obtained from Eqs. 9 and 10, allowing us to calculate the inlet conditions for Eqs. 5 and 6.

Fully Developed Flow Model. Another model, referred to here as the fully developed flow model applicable for a fully developed riser flow, does not include the momentum balance equations. Instead, the slip velocity u_{sl}, defined as the difference between the gas and solid phase velocities, is equated to the terminal settling velocity u_t, as shown in Eq. 11, with related expressions given in Eqs. 12 and 13. Substitution of Eqs. 12 and 13 in Eq. 11 results in a quadratic expression from which the solution for the void fraction ϵ_g is obtained, as shown in Eq. 14. The superficial velocities $u_{s,g}$ and $u_{s,s}$ are related to the gas and solid flow rates, as shown in Eqs. 15 and 16. The terminal settling velocity is calculated from Eq. 17.

$$u_{sl} = u_t = u_{i,g} - u_{i,s} \tag{11}$$

$$u_{i,g} = u_{s,g}/\epsilon_g \tag{12}$$

$$u_{i,s} = u_{s,s}/\left(1-\epsilon_g\right) \tag{13}$$

$$\epsilon_g = \frac{\left(u_t+u_{s,g}+u_{s,s}\right) - \sqrt{\left(u_t+u_{s,g}+u_{s,s}\right)\left(u_t+u_{s,g}+u_{s,s}\right) - 4u_{s,g}u_t}}{2u_t} \tag{14}$$

$$u_{s,g} = F_g/\left(A\rho_g\right) \tag{15}$$

$$u_{s,s} = G_s/\left(A\rho_s\right) \tag{16}$$

$$u_t = \sqrt{\frac{4gd_p\left(\rho_s-\rho_g\right)}{3\rho_g C_D}}. \tag{17}$$

Therefore, for ϵ_g Eq. 14 replaces the solid-phase momentum balance equation Eq. 6 of the one-dimensional hydrodynamic model. Since Eq. 14 is an algebraic equation, no inlet condition for ϵ_g is required in this model. Moreover, in the present study the pressure drop across the entire riser length is very small (< 300 Pa). Hence, in the riser the pressure is assumed constant and equal to the inlet pressure. Consequently, the gas-phase momentum balance equation Eq. 5 is also omitted in the fully developed flow model. The remaining equations and inlet conditions are identical to those of the one-dimensional hydrodynamic model described previously.

Rate Equations

The kinetic model for simultaneous SO_2–NO_x adsorption is based on the results of an experimental investigation in a fixed-bed reactor (De Wilde et al., 2000). Table 2 summarizes the reactions involved in the simultaneous adsorption of SO_2 and NO_x. Both SO_2 and NO_2 adsorb independently on the free sites of the sorbent surface via steps S1 and S2, leading to SO_2^* and NO_2^*. The SO_2^* species further interacts with another free site via step S3 to form SO_2^{**}, upon which the NO and O_2 are simultaneously adsorbed (S4) on a much shorter time scale. This is followed by the association of many SO_2^* and O_2, leading to the complex $R_t^{\beta *}$, and subsequently $R_s^{\beta *}$ via paths P1 and P2. The adsorbed NO_2^* acts as a new site for additional adsorption of SO_2 (path P3). However, free NO_2 in the gas phase promotes the disintegration of the complex $R_t^{\beta *}$ and releases large quantities of NO and O_2 (path P4).

The following extensions are made to the model proposed by DeWilde et al. (2000) in order to apply the kinetic model to the continuous GSA riser. The corresponding values of the kinetic parameters, as used in the present model, are summarized in Table 2.

1. A gas-phase oxidation step (S5) for NO is introduced as follows:

$$NO + 1/2O_2 \rightarrow NO_2.$$

This reaction is in fact reversible. However, at the low temperatures (373–423 K) prevalent in the GSA, the dissociation of NO_2 is negligible. The rate of this reaction is very slow as such. Since the gas-phase residence time in the laboratory fixed-bed microreactor is very low (< 0.02 s), it was not con-

Table 2. Reaction Steps/Paths and Kinetic Parameters Considered in the Kinetic Modeling of SO_2–NO_x Adsorption on Na/γ–Al_2O_3

Reaction Step/Path	Elementary Reaction Steps/ Lumped Reaction Path	Sites Per Mol Species	Kinetic Parameters[§]	
			$k_i^{\ddagger\ddagger}$	$E_i^{\ddagger}$
S1	$SO_2 + * \overset{k_1}{\rightarrow} SO_2^*$	1	4.21[##]	5.73
S2	$NO_2 + * \overset{k_2}{\rightarrow} NO_2^*$	1	2.25[##]	2.32
S3	$SO_2^* + * \overset{k_3}{\rightarrow} SO_2^{**}$	2	2.63[†]	7.80
S4	$NO + O_2 + SO_2^{**} \overset{k_4}{\rightarrow} [(NO_2)(SO_3)]^* +$	1	2052.0[††]	1.2
P1	$[(NO_2)(SO_3)]^* + \{(\beta-1)SO_2^*, \alpha O_2\} \overset{k_5}{\rightarrow} R_t^{\beta *}$	β	65.0[†]	2.58
P2	$R_t^{\beta *} + O_2 + \{0.5\ O_2\} \overset{k_6}{\rightarrow} R_s^{\beta *}$	β	0.048[##]	35.81
P3	$NO_2^* + SO_2 + \{2SO_2\} \overset{k_7}{\rightarrow} NO + [O(SO_2)_3]^*$	1	0.79[##]	46.34
P4	$NO_2 + R_t^{\beta *} \overset{k_8}{\rightarrow} 2NO + 4O_2 + Q^{\beta *}$	β	0.80[##]	37.92
S5	$NO + 1/2O_2 \overset{k_9}{\rightarrow} NO_2$	—	0.52[§§]	10.0

Note: $C_t = 0.93^{\#,\|}$ & $0.41^{\#,\|\|}$; $g = 8.0$.

[#] $mol_{site}kg^{-1}_{sorbent}$. [‡‡] at 387 K.

[##] $m^3\ mol^{-1}_{site}\ s^{-1}$. [§] real surface model.

[†] $m^3\ mol^{-1}_{site}\ s^{-1}$. [§§] $m^{4.5}\ mol^{-0.5}\ mol^{-1}_{site} s^{-1}$.

[††] $m^6\ mol^{-1} mol^{-1}_{site}\ s^{-1}$. [‖] Sorbent A.

[‡] $kJ\ mol^{-1}$. [‖‖] Sorbent B.

sidered in the development of the original kinetic model. For the GSA riser, the gas residence time is much higher (5 s), which makes the inclusion of this step necessary. The reaction-rate parameters of this step are obtained from the NO_2 data of the GSA riser pilot plant. The rate equation for this step is written as

$$r_9 = k_9 C_{NO} C_{O_2}^{0.5} \theta_n, \tag{18}$$

where θ_n is the Elovich factor for a nonuniform surface model:

$$\theta_n = \exp(-g\theta_c), \tag{19}$$

where g is a constant ($= 8.0$), as reported by De Wilde et al. (2000), and θ_c is the fractional cumulative site coverage. The latter is defined as the fraction of covered sites per mole of total sites:

$$\theta_c = \sum_j \beta_j \theta_j, \tag{20}$$

where θ_j is the fractional coverage of the species j and β_j indicates the number of active sites covered per mole of surface species j.

An alternative rate expression without θ_n and different value of the rate coefficient k_9, also adequately simulates the pilot-plant data. This indicates that the preceding reaction occurs primarily in the gas phase. However, in both of these cases, the reaction rate was found to be two orders of magnitude higher than the corresponding value obtained from the known homogeneous gas-phase reaction kinetics. The higher rate of this reaction in the GSA is attributed to the promoting effect of (a) the presence of water in the flue gas (Mok and Ham, 1998), and (b) the availability of sufficient free sites * due to the continuous supply of the regenerated sorbent. The second argument is strengthened from the fact that in the GSA pilot riser, NO_2 is not produced if the regenerated sorbent flow is stopped.

2. The k_2 value for the NO_2 adsorption (step S2 of Table 2), that is, 2.25 $m^3 \cdot mol^{-1}_{site} \cdot s^{-1}$, is based on the NO_2 data of the GSA pilot plant. The k_2 of the original kinetic model of De Wilde et al. (2000), represents a case with substantial NO_2 concentration ($> 2{,}000$ ppm) in the inlet flue gas. However, when the inlet NO_2 concentration is very small (< 100 ppm), the rate of NO_2 adsorption is much slower than expected from the kinetics obtained at high NO_2 concentrations. Actually, an increase in the gas-phase NO_2 concentration in the GSA riser is observed, as is discussed in the section titled "Comparison of Simulated Data with GSA Pilot-Plant Data.

3. The stoichiometric coefficients ($\beta - 1$) and α of path P1 (Table 2) are, respectively, 3 and 1.5 per mole of $[(NO_2)(SO_3)]$, and the rate coefficient k_5 amounts to 65.2 $m^3 \cdot mol^{-1}_{site} \cdot s^{-1}$, based on the GSA riser data. Path P1 is not elementary, but consists of multiple consecutive steps. For such a path, the kinetic parameters may not remain constant over a very wide range of operating conditions. For example, the inlet SO_2 concentration in the laboratory fixed-bed reactor is about 20 times higher than those in the GSA riser. Only a model that accounts fully for the elementary steps involved in path P1 can describe such a large variation in SO_2 concentration without altering the kinetic parameters. Furthermore, to avoid corrosion, the fixed-bed kinetic experiments were conducted with moisture-free gas, in contrast to the large amount of water in the GSA inlet gas.

4. The total concentration of adsorption sites C_t of Sorbent-A (fresh) for the GSA riser was found to be the same as the estimated value in the kinetic model (De Wilde et al., 2000), that is, 0.928 $mol_{site} \cdot kg^{-1}_{sorbent}$. It may be noted that the kinetic study is also based on Sorbent-A. However, for Sorbent-B, that is, the equilibrated sorbent, C_t was found to be lower (0.408 $mol_{site} \cdot kg^{-1}_{sorbent}$) as expected, based on the GSA

pilot-plant data. The remaining kinetic parameters are identical for both sorbents.

Numerical Solution

Solution methodology

Besides the i concentrations of the gas-phase components C_i (without inert) and j coverages of surface species θ_j, the dependent variables in the model are ϵ_g, P, u_g, and u_s. Equations 1 to 4 have the property that the righthand sides could be explicitly calculated, and hence explicit Euler or Runga-Kutta integration methods could be easily adopted (Gear, 1971). However, the righthand sides of Eqs. 5 and 6 contain the derivatives of a dependent variable, namely pressure. For the ease of solution, first Eqs. 5 and 6 are added and rearranged, leading to a differential equation, Eq. 21, with pressure P, and Eq. 22, with ϵ_g, as dependent variables. Hence, in the one-dimensional hydrodynamic model, Eqs. 5 and 6 are replaced by Eqs. 21 and 22.

Total Pressure Drop

$$-A\frac{dP}{dz}=\frac{d}{dz}\left(\epsilon_g\rho_g u_g^2 A\right)+\frac{d}{dz}\left[\left(1-\epsilon_g\right)\rho_s u_s^2 A\right]+A\epsilon_g\rho_g g + A\left(1-\epsilon_g\right)\rho_s g - A\left(F_{w,g}+F_{w,s}\right) \quad (21)$$

Explicit Equation for ϵ_g

$$-\frac{d}{dz}\left[\left(1-\epsilon_g\right)\rho_s u_s^2 A\right]+\left[\left(1-\epsilon_g\right)/\epsilon_g\right]\frac{d}{dz}\left[\epsilon_g\rho_g u_g^2 A\right] + \left[\left(1-\epsilon_g\right)/\epsilon_g\right]\beta A(u_g-u_s)+\left(1-\epsilon_g\right)A\rho_g g - \left[\left(1-\epsilon_g\right)/\epsilon_g\right]AF_{w,g}+\beta A(u_g-u_s)-A\left(1-\epsilon_g\right)\rho_s g + AF_{w,s}=0. \quad (22)$$

The model equations are ordinary differential equations of the initial-value type, and these are integrated using the Euler backward difference technique, with a large number of incremental steps ($N=1000$) in the axial direction.

First, Eqs. 3 and 4 are integrated to obtain the values of F_g and G_s for the nth grid. Backward discretization of Eq. 22 results in a nonlinear algebraic equation for ϵ_g, which is solved using the Regula-Falsi method (Lapidus, 1962). The values of u_g , u_s, and P are calculated from Eqs. 9, 10 and 21 inside the Regula-Falsi loop with the iterative value of ϵ_g. Finally, Eqs. 1 and 2 are integrated for all the C_i and θ_j, since the values of ϵ_g, P, u_g, and u_s for the grid n are now known.

Recycle-loop convergence

The initial values for the species coverages of the recycle sorbent are assumed. The coverages of the combined sorbent are calculated from Eq. 8. The riser is simulated with these calculated species coverages at the inlet. The convergence of the recycle loop is verified using the SO_2 concentration between two subsequent iterations with a tolerance of <0.5 ppm, since SO_2, among all the responses to any variation in the species coverages, is the most sensitive. The numerical code is written in Fortran-77 and takes about 30-s CPU time on a Solaris 2.4 Sun SPARC system, for the simulation of a set with 50 experimental data points.

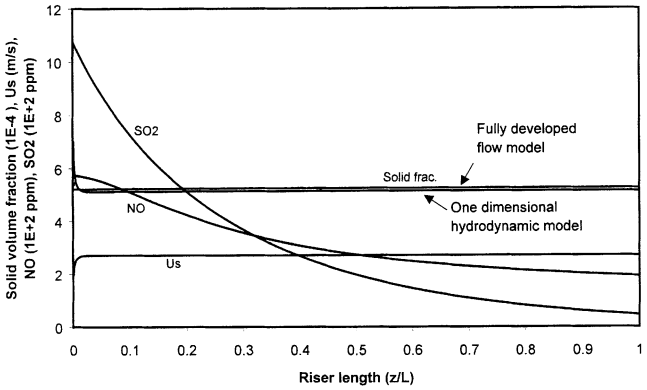

Figure 2. Solid-volume fraction, solid velocity, outlet NO, and SO_2 concentrations as a function of riser length for two riser models.

In the fully developed flow model, ϵ_g is calculated using Eq. 14. For the one-dimensional hydrodynamic model, ϵ_g is obtained from Eq. 22. The NO and SO_2 responses coincide for both the models. Inlet SO_2 and NO concentrations are 1072 and 584 ppm. The inlet gas flow rate is 4.36 Nm^3/s.

Comparison of Hydrodynamic Models

As described in the third section, the present work employs the one-dimensional hydrodynamic model and the fully developed flow model. Figure 2 shows the axial variations of the solid volume fraction $(1-\epsilon_g)$, solid velocity u_s, NO, and SO_2 concentrations at the riser outlet for Sorbent-A with the preceding two models. The fully developed flow model predicts a nearly constant profile for the solid fraction $(1-\epsilon_g)$. However, the one-dimensional hydrodynamic model shows a short acceleration zone at the riser bottom where the solid volume fraction is sharply reduced to that of the fully developed flow model. In both the models, the solid volume fraction for most of the riser is nearly identical and amounts to 5×10^{-4}, which indicates a very dilute riser flow for the GSA. Similarly, for the one-dimensional hydrodynamic model, the solid velocity at the beginning increases sharply, indicating the initial acceleration zone. However, the length of the initial acceleration zone is too short to have any impact on the amount of SO_2 and NO adsorbed. Hence, the SO_2 and NO concentrations coincide for both the models.

Comparison of Simulated Data with GSA Pilot-Plant Data

Parity diagrams of NO_x, SO_2, and NO_2

Figures 3a, 3b, and 3c show the parity diagrams of NO_x, SO_2, and NO_2 concentrations at the riser outlet for Sorbent-A and Sorbent-B, covering about 700 data points. These data include the period of startup and the regions of unsteady fluctuations. It is seen that the model predicts the NO_x ($=$ NO + NO_2) concentration quite accurately over a broad range of concentrations. The SO_2 and NO_2 concentrations are also predicted adequately, but with a relatively higher scatter than NO_x. It can be noted that the scales of the SO_2 and NO_2 diagrams are smaller than that for NO_x. In the parity diagrams, the points that are far away from the expected diagonal line mainly correspond to the unsteady operation of

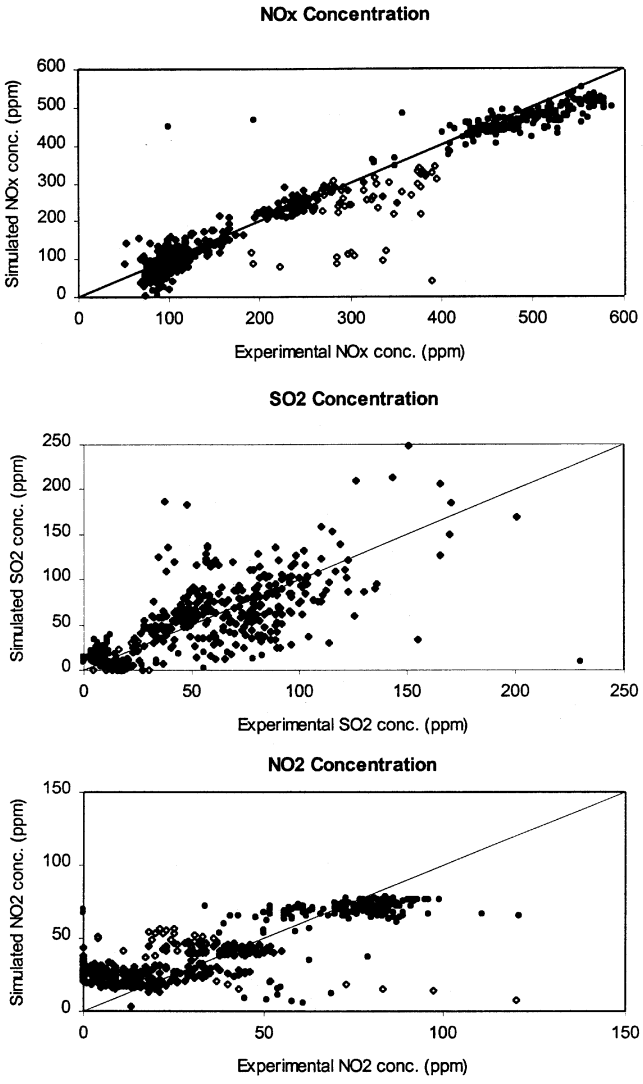

Figure 3. Parity of steady-state NO_x, SO_2, and NO_2 responses at riser outlet with sorbents A and B in continuous GSA pilot-plant operation.

Simulated values are obtained by using Eqs. 1–4 and Eqs. 21–22 and inlet conditions given by Eqs. 7–10. Markers: ◆—sorbent A; ◇—sorbent A unsteady; ●—sorbent B.

the pilot plant with Sorbent A (unfilled diamonds). Moreover, since NO_2 is generated by the gas-phase oxidation of NO via step S5, it is felt that continuous measurement of the inlet O_2 concentration is essential for a more accurate simulation of the NO_2 response. The present simulation has been performed assuming a constant value of 10 ppm inlet NO_2 concentrations and 20,000 ppm of inlet O_2 concentration.

Steady-state SO_2 and NO removal efficiencies

Figure 4 shows a comparison between the simulated and experimental SO_2 and NO removal efficiencies for Sorbent-B, based on about one hundred steady-state data points. The removal efficiency is defined as % (inlet−outlet)/inlet concentration. The inlet SO_2/NO ratio is also shown in Figure 4.

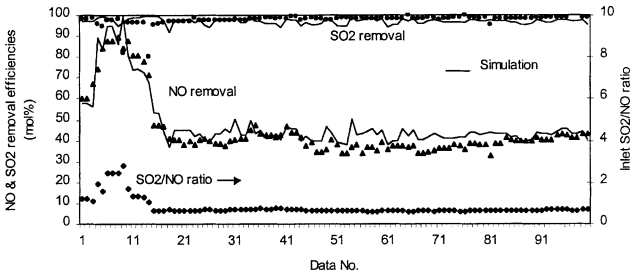

Figure 4. Steady-state NO and SO_2 removal efficiencies in a continuous operation with sorbent B.

Bold lines indicate simulation results and points are experimental data. The removal efficiencies are calculated from the outlet concentrations obtained by using Eqs. 1–4 and Eqs. 21–22 and inlet conditions given by Eqs. 7–10.

In addition, other process variables are simultaneously altered in these experimental data, but the variation in the inlet SO_2/NO ratio is the major one.

In Figure 4, it is seen that the model adequately follows the experimental responses for both SO_2 and NO removal efficiencies. In the beginning (< 25 data points), the NO removal efficiency has significantly improved from the 60% to the 90% level, mainly due to an increase in the inlet SO_2/NO ratio from 1.2 to 2.8. Subsequently, the NO removal efficiency decreases with a corresponding decrease in the inlet SO_2/NO ratio. On the other hand, the SO_2 removal efficiency has been consistently above 95% for both the experimental and simulated values. Certain undesirable spikes in the SO_2 simulation are mainly due to the difficulty in accurately estimating the sorbent flow rates from the riser pressure drop data, as discussed in the second section.

Figure 4 clearly demonstrates the ability of the SNAP process to simultaneously remove both NO and SO_2 at a high level of efficiency. A similar effect of the inlet SO_2−NO ratio on the NO removal is also observed for Sorbent-A.

Evolution of Process Variables Across Riser Length

As discussed in the section titled "Comparison of Hydrodynamic Models," Figure 2 shows the axial evolution of some dependent variables across the riser length. It is observed that at the bottom section of the riser, the concentration of SO_2 decreases much faster than does that of NO. This is because SO_2 can directly adsorb on the sorbent free sites, whereas NO can adsorb only if SO_2^{**} species is formed (step S3 in Table 2). Also, beyond 70% riser height, changes in both SO_2 and NO concentrations are very small, which is due to the decrease in the concentration of free sites near the end of the riser.

Conical bottom riser

Figure 5 shows the gas velocity u_g, solid velocity u_s, solid fraction $(1-\epsilon_g)$, NO, and SO_2 concentrations at the riser bottom section for a cylindrical- and a conical-bottom riser. The inlet conditions are identical to those used in the sixth section, and the one-dimensional hydrodynamic model is used for simulation. It is seen that the gas velocity u_g for the coni-

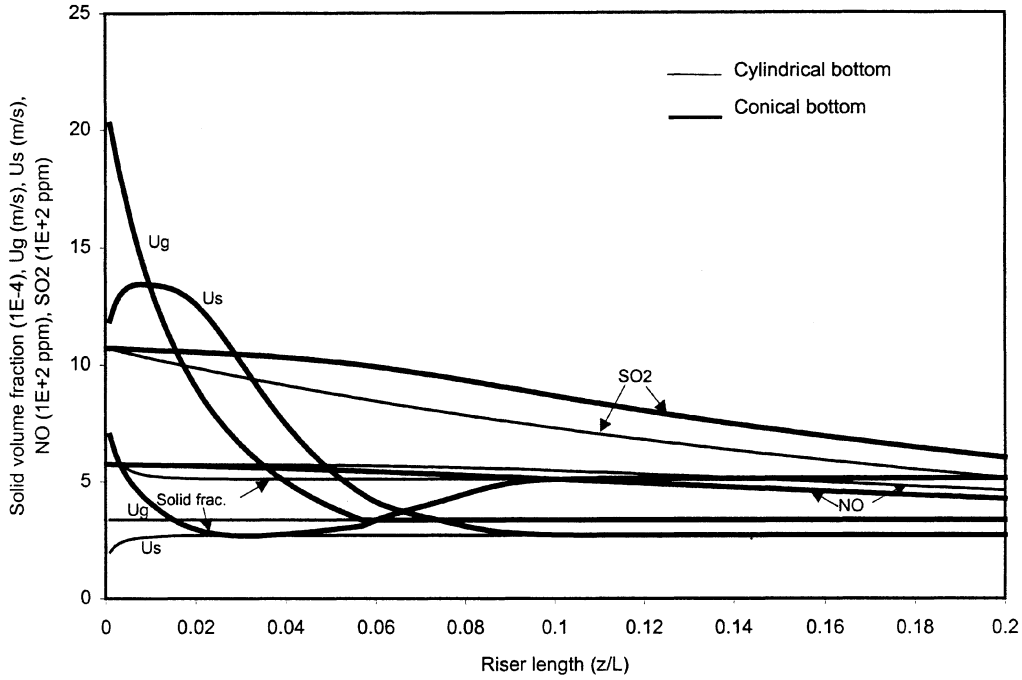

Figure 5. Solid-volume fraction, gas and solid velocities, NO, and SO_2 concentrations as a function of axial length for different riser bottom geometry.

Bold lines represent the conical bottom and thin lines correspond to the cylindrical bottom riser. The inlet angle of the cone is 60° horizontal and the length of the conical section is 0.8 m.

cal bottom is very high (> 20 m/s) at the riser bottom and gradually reduces to the corresponding value of 3.3 m/s for the cylindrical-bottom riser due to the increase of the cross-sectional surface area. The solid velocity u_s for the cylindrical riser increases at the beginning due to the normal acceleration of the sorbent. In the conical-bottom case, however, u_s initially increases due to the acceleration, then passes through a maximum before sharply decreasing in parallel with the gas velocity.

The much higher u_g and u_s in the conical bottom result in a lower solid volume fraction $(1-\epsilon_g)$ of 2.7×10^{-4} as compared to 5.1×10^{-4} for the cylindrical-bottom riser. The lower solid fraction, along with the lower cross-sectional area in the conical riser, result in a lower amount of SO_2 and NO adsorption, leading to higher concentrations of these components in the gas phase. The effect is more important for SO_2 than for NO. Thus at the end of the conical section (at $z/L = 0.1$), the SO_2 removal efficiency is 18.7% compared to 31.5% for a cylindrical-bottom riser. However, these differences narrow down at the end of the riser. Moreover, due to the higher velocity of the incoming flue gas, a conical-bottom riser is desirable as a more efficient conveyer of the sorbent at the riser bottom.

Effect of Inlet SO_2–NO Ratio on Removal Efficiencies

Figure 6 shows the effect of the inlet SO_2–NO ratio on the removal efficiencies of SO_2 and NO. It is seen that the inlet SO_2–NO ratio has a strong positive effect on the NO and NO_x removal efficiencies. The final results are different, however, depending on the way the inlet SO_2–NO ratio is altered.

When the inlet SO_2 concentration is increased at a constant inlet NO concentration, the SO_2 removal efficiency decreases beyond a certain inlet SO_2–NO ratio. This is because SO_2 adsorption requires free sites (step S1 in Table 2), and if the latter are not sufficiently available, breakthrough of SO_2 occurs. On the other hand, if the inlet NO concentration is varied at a constant inlet SO_2 concentration, the SO_2 removal efficiency does not change, since there is no net consumption of free sites in the NO adsorption.

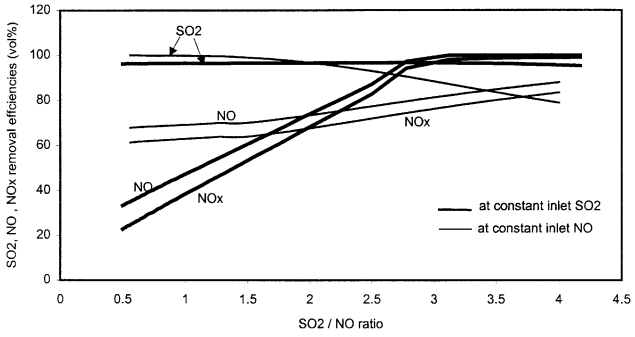

Figure 6. SO_2, NO, and NO_x removal efficiencies as a function of inlet SO_2/NO ratio at a constant inlet NO or SO_2 concentration.

Bold lines are obtained at a constant inlet SO_2 concentrations of 1000 ppm and thin lines correspond to the constant inlet NO concentration of 500 ppm. Inlet concentration of NO_2 is kept constant at 10 ppm in both cases.

The NO removal efficiency is very different, depending on how the inlet SO_2–NO is varied. For example, for a constant inlet NO concentration, it is very difficult to achieve complete NO removal even if the inlet SO_2–NO ratio is very high (> 4), unless additional free sites are supplied. This is because in this case, the SO_2 removal efficiency is decreased at higher inlet SO_2–NO ratios. Hence, for a complete NO removal it is essential to not only have a higher inlet SO_2–NO ratio, but also to ensure the availability of sufficient free sites. The latter is essential for the adsorption of the gas-phase SO_2 to form SO_2^*, and subsequently SO_2^{**} (step S3 in Table 2), so that additional NO is adsorbed.

On the other hand, the inlet SO_2–NO ratio has a more pronounced effect on the NO removal if the inlet NO concentration is altered at a constant inlet SO_2 concentration. This, of course, implies a lower inlet NO concentration at a higher inlet SO_2–NO ratio. Since the inlet concentration of SO_2 is not changed, the SO_2^{**} concentration in the surface remains constant, and thus the absolute value of NO is adsorbed. However, the NO removal efficiency increases, since the inlet NO concentration is lower at a higher inlet SO_2–NO ratio.

Regarding the NO_2 adsorption, Figure 6 indicates that the inlet SO_2–NO ratio at a constant inlet SO_2 concentration affects the NO_x removal efficiency more than it does that of NO. This effect is, however, not visible if the inlet SO_2–NO ratio is altered at a constant inlet NO concentration. In the former case, since the inlet NO concentration is decreased while increasing the inlet SO_2–NO ratio, less NO_2 is generated from the gas-phase oxidation of NO via step S5. Thus, when the concentration of NO_2 at the riser inlet is negligible, the conditions that favor NO removal also improve the removal efficiencies of NO_2 and NO_x. Hence, a higher inlet SO_2–NO ratio is always desirable for achieving maximum NO and NO_x removal. However, if the inlet SO_2 concentration is increased, it also is necessary to increase the regenerated sorbent flow rate in order to maintain the SO_2 removal efficiency at the maximum level.

Effect of Sorbent Flow Rates on Removal Efficiencies and Surface Coverages

In this section, the regenerated and the recycle sorbent flow rates are varied one at a time. This is different from the previous simulations where these flow rates are obtained from the set riser pressure drop and the inlet gas flow rate.

Figure 7 shows the variations in the NO and SO_2 removal efficiencies after separately decreasing the *regenerated* and the *recycle* sorbent flow rates to one-fourth of their normal values. First the *regenerated* sorbent flow rate is decreased from 1.02 kg/s to 0.26 kg/s (zone I). After the convergence is reached, this is reset to its initial value (zone II). Thereafter, the *recycle* sorbent flow rate is decreased from 3.07 kg/s to 0.77 kg/s (zone III). Figure 7 also shows the cumulative site coverage θ_c and the Elovich factor θ_n.

The convergence of the recycle loop is monitored by introducing the *cumulative sorbent residence time* in the riser. The latter is obtained by multiplying the single-pass sorbent residence time in the riser by the number of passes made by the recycle stream, that is, the number of iterations made during the recycle-loop convergence. As shown in the Appendix, this provides a measure of the residence time distribution of the sorbent in the riser, particularly when the variation in the species coverages due to reactions in different passes, as shown in Eq. A11 is negligible.

Regenerated sorbent flow rate

Figure 7 shows that the regenerated sorbent flow rate has a major effect on both the SO_2 and the NO removal efficien-

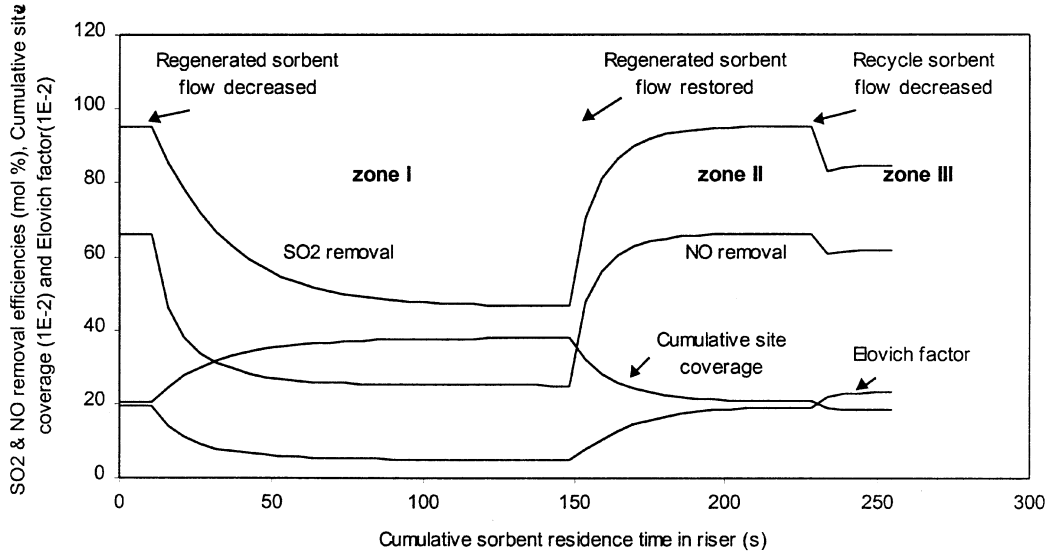

Figure 7. SO_2 and NO removal efficiencies, cumulative site coverage θ_c, and Elovich factor θ_n as a function of the regenerated and recycle sorbent flow rates.

Regenerated sorbent flow rate is varied from 1.02 kg/s to 0.25 kg/s (zone I) and restored back to 1.02 kg/s, as shown in zone II. Recycle sorbent flow rate is changed from 3.07 kg/s to 0.77 kg/s in zone III.

cies. The NO removal efficiency drops from 67% to 24% and the SO_2 removal efficiency drops from 96% to 52% when the flow rate decreases by a factor of 4. Correspondingly, the cumulative site coverage, θ_c, increases from 0.21 to 0.38, but more importantly, the Elovich factor θ_n decreases exponentially from 0.19 to 0.05, as given by Eq. 19. The decrease in the adsorption rates (De Wilde et al., 2000) is proportional to the latter, leading to less SO_2 adsorption, and hence, lower SO_2^{**} coverage and also lower NO removal. Thus the regenerated sorbent flow rate is a very important variable for GSA.

Recycle sorbent flow rate

In Figure 7, although the change in the recycle sorbent flow rate (zone III) is in fact three times the change introduced previously for the regenerated sorbent flow rate, the effect of the former on the removal efficiencies is not so pronounced. For example, the SO_2 removal efficiency has dropped from 96% to 83% and the NO removal efficiency has decreased from 66% to 60%. Similarly, the variations in θ_c and θ_n are also smaller.

The mild effect of the recycle sorbent flow rate is due to (1) a partly covered surface of the recycle sorbent by various species, and (2) the backmixing of the sorbent phase at higher recycle ratio. Concerning the first point, the higher recycle rate only helps to saturate the remaining free sorbent sites primarily with additional adsorption of SO_2. Hence, the improvement in SO_2 removal is somewhat better than in NO removal. In Figure 7, although the cumulative site coverage θ_c is not so high (≈ 0.21), the Elovich factor θ_n is rather small (≈ 0.19), due to the exponential dependence on θ_c. Hence, the recycling of the sorbent is only useful if the used sorbent has substantial residual adsorption activity, indicated by a higher value of θ_n.

As regards the backmixing effect, it is seen in Figure 7 that the recycle-loop convergence is much faster when the recycle sorbent flow rate is lower (zone III) or the regenerated sorbent flow rate is higher (zone II). In other words, a lower recycle ratio helps in a faster convergence of the surface species coverages. This can be better understood by looking at the mean residence time of the sorbent t_s in the riser for the conditions just mentioned. For a fully developed riser flow with negligible slip, the mean residence time of the sorbent τ_s can be expressed as

$$\tau_s = \tau_g(1 + R_c) \tag{23}$$

$$R_c = \text{recycle ratio} = G_{s,rc}/G_{s,rg},$$

where τ_g is the gas-phase mean residence time, and $G_{s,rc}$ and $G_{s,rg}$ are the recycle and regenerated sorbent flow rates. Thus, for zones I, II, and III, the recycle ratios R_c are 12, 3, and 0.75, and the corresponding τ_s values are 69 s, 21.2 s, and 9.3 s, respectively, with a τ_g of 5.3 s. As expected, a higher recycle ratio introduces significant backmixing in the plug-flow riser, indicated by a longer convergence time in zone I. In contrast, a lower recycle ratio leads to a faster convergence of the species coverages, as seen in zone III.

Steady-state species coverages of the sorbent

Table 3 summarizes the steady-state species coverages of the used sorbent at different regenerated and recycle sorbent flow rates. The first column in Table 3 corresponds to the flow rates at normal operation, with a recycle ratio of three. The second and the third columns correspond to very low flow rates of the regenerated or recycle sorbent.

In a normal operation, the cumulative site coverage θ_c indicates that about 80% of the sites are still free. However, the Elovich factor θ_n is only 0.19, indicating a lower real surface activity. In fact, in the third column with very low recycle sorbent flow, θ_c and θ_n are very close to those for the normal operation. Hence, by recycling, only marginal changes occur in the cumulative site coverage, θ_c. However, when the regenerated sorbent flow is very low (second column), θ_c increases to a very high value due to the nonavailability of sufficient free sites. Consequently, the sorbent becomes fully saturated ($\theta_n \approx 0$) after some time if the regenerated sorbent flow is stopped.

The coverage of SO_2^* species is very different for the preceding operations. Interestingly, for the low recycle sorbent flow, the coverage of SO_2^* is higher than that for the normal operation. However, the SO_2^* coverage is much higher when the regenerated sorbent flow is very low. Thus there is an

Table 3. Steady-State Species Coverages of the Recycle Sorbent for Different Riser Operations

	Normal Operation	Very Low Regenerated Sorbent Flow Rate	Very Low Recycle Sorbent Flow Rate
Input			
Regenerated sorbent flow rate, kg/s	1.02	0.003	1.02
Recycle sorbent flow rate, kg/s	3.06	3.06	0.003
Output			
Species coverage, $\theta_j(\times 10^{-4})$			
SO_2^*	8.0	120.0	24.5
NO_2^*	96.3	0.76	42.0
SO_2^{**}	0.7	0.06	2.5
$[(NO_2)(SO_3)]^*$	138.0	2.4	260.3
$R_f^{\beta *}$	255.0	32.0	292.0
$R_s^{\beta *}$	191.0	1649.0	37.9
$[O(SO_2)_3]^*$	15.8	161.0	1.5
$Q^{\beta *}$	6.5	26.1	1.1
$\theta_c(\times 10^0)$	0.21	0.71	0.17
$\theta_n(\times 10^0)$	0.19	0.003	0.27

optimum recycle ratio at which the coverage of SO_2^* is minimum. It may be noted that SO_2^* plays a crucial role in the adsorption of NO by forming the desired species SO_2^{**}. However, a large amount of SO_2^* is also consumed in the formation of the complex $R_t^{\beta *}$ via path P1. Hence, for maximum NO removal, it is desirable to minimize the rate of path P1 so that the rate of steps S3 and S4 are enhanced. From this point of view, an operation that leads to the maximum $[(NO_2)(SO_3)]^*$ via step S4 and minimum SO_2^* is the most desirable one for NO adsorption.

The preceding phenomenon becomes clearer when the coverages of $[(NO_2)(SO_3)]^*$ and $R_t^{\beta *}$ are compared. At lower recycle sorbent flow, the coverage of the former species is much higher than in the normal operation, due to the relatively lower mean residence time t_s of the sorbent in the riser, as seen from Eq. 23. If τ_s is increased by increasing the recycle ratio to 3, as in the normal operation, the species $[(NO_2)(SO_3)]^*$ is converted to $R_t^{\beta *}$, and subsequently to $R_s^{\beta *}$ via paths P1 and P2. Since a large amount of SO_2^* is consumed in path P1, this results in the lowest coverage of SO_2^* for the normal operation (first column). However, it is seen that the complex formation is still very high in the normal operation. Hence, the optimum recycle ratio lies somewhere between 0 and 3.

Subsequently, with a very low regenerated sorbent flow, SO_2^* again increases due to the lower SO_2^{**} formation rate (step S3), as seen by the very small value of SO_2^{**} resulting from the nonavailability of enough free sites. This operation provides an extreme situation where most of the reactions are driven toward completion. Thus, higher concentrations of all the stable species such as $R_s^{\beta *}$, $[O(SO_2)_3]^*$ and $Q^{\beta *}$ result.

Conclusions

A steady-state one-dimensional hydrodynamic model is implemented for the simultaneous adsorption of SO_2-NO_x in a riser configuration. The model consists of the continuity and the momentum balance equations for the gas and solid phases using a two-fluid continuum approach. In addition, the continuity equations for the gas-phase components and surface species are also solved. The rate equations of the different reactions are based on the kinetic model of De Wilde et al. (2000), extended for application to the riser configuration.

Simulation results are validated by the continuous experimental data obtained from a riser pilot installation of a flue-gas capacity of 4.2 Nm^3/s. The model simulations are in good agreement with the pilot-plant data over a broad range of conditions. However, the horizontal banding in the NO_2 parity plot is mainly due to the assumption of constant O_2 concentration at the riser inlet for all the experiments. A hydrodynamic simulation of the riser indicates that the initial acceleration zone at the riser bottom is very short due to an extremely dilute riser flow in the gas suspension adsorber with a solid fraction less than 7.0×10^{-4}. Hence, we can safely consider the flow in such a dilute phase riser to be fully developed.

The SO_2 adsorption is very rapid in the bottom of the riser due to the availability of sufficient free sites. However, the adsorption of NO and SO_2 slow down considerably after about 70% of the riser length. Since NO_2 is generated inside the riser due to the gas-phase oxidation of NO, the conditions that favor NO adsorption also result in a lower concentration of NO_2.

The inlet SO_2-NO ratio has a profound effect on the NO adsorption in particular. It is observed that, for a constant inlet SO_2 concentration, increasing this ratio considerably improves the NO and NO_x removal efficiencies. However, if this ratio is altered at a constant NO concentration, the effect on NO removal is less prominent, due to a simultaneous drop in the SO_2 removal efficiency. In the latter case, it is desirable to increase the regenerated sorbent flow rate for the adsorption of the additional SO_2 supplied at the riser inlet.

The model corroborates the pilot-plant observation that the regenerated sorbent flow rate is an important variable in the simultaneous adsorption of SO_2-NO_x. Recycling the sorbent helps to a limited extent in adsorbing additional SO_2. There is an optimum recycle ratio at which the adsorbed SO_2 species and the remaining free sites of the recycle sorbent are best utilized for improving the removal efficiencies of SO_2 and NO. Hence, with suitable conditions in the riser adsorber, it is possible to achieve simultaneous SO_2 removal above 95% and NO removal above 80%.

Acknowledgment

This work was financed by the European Commission within the frame of the Thermie project under Contract No. SF 243/98 DK/BE/UK (project partners: Laboratorium voor Petrochemische Techniek-Universiteit Gent, FLS miljo a/s—Denmark & Howden Air & Gas Division—UK). Two of the authors (G. H. and G. B. M.) are grateful to the "Fonds voor Wetenschappelijk Onderzoek-Vlaanderen" (FWO-N) for financial support.

Notation

A = cross-sectional surface area of the riser, m^2
C_i = gas-phase concentration of the component i, $mol\cdot m_{gas}^{-3}$
C_D = drag coefficient for an isolated particle
D = riser diameter, m
C_t = site capacity of the sorbent, $mol_{total\ site}\cdot kg_{sorbent}^{-1}$
d_p = particle diameter, m
F_g = volumetric flue gas flow rate, $m^3\cdot s^{-1}$
$F_{w,g}$ = volumetric wall frictional force acting on the gas phase ($N\cdot m^{-3}$ gas–solid mixture)
$F_{w,s}$ = volumetric wall frictional force acting on the solid phase ($N\cdot m^{-3}$ gas–solid mixture)
f_g, f_s = friction factors for gas and solid phases, dimensionless
g = gravitational force per unit mass, $m\cdot s^{-2}$
G_s = total sorbent flow rate, $kg\cdot s^{-1}$
$G_{s,rc}$ = recycle total sorbent flow rate, $kg\cdot s^{-1}$
$G_{s,rg}$ = regenerated sorbent flow rate, $kg\cdot s^{-1}$
M_i = mol. wt. of component i
P = total pressure, $kg\cdot m^{-1}\cdot s^{-2}$
Re_p = particle Reynolds number $= \rho_g u_g d_p/\mu$, dimensionless
R_e = Reynolds number $= \rho_g u_g D/\mu$, dimensionless
R_i = net production rate of the component i in the gas phase, $mol\cdot mol_{site}^{-1}\cdot s^{-1}$
R_j = net production rate of the species j, $mol\cdot mol_{site}^{-1}\cdot s^{-1}$
R_c = recycle ratio, dimensionless
u_g = interstitial gas velocity, $m_{gas}^3\cdot m_{reactor}^{-2}\cdot s^{-1}$
u_s = interstitial solid velocity, $m_{gas}^3\cdot m_{reactor}^{-2}\cdot s^{-1}$
u_t = terminal settling velocity of a single particle, $m\cdot s^{-1}$
u_{sl} = slip velocity, $m\cdot s^{-1}$
V_r = volume of riser, m^3
z = axial length of the riser, m

Greek letters

θ_c = fractional cumulative site coverage, $\text{mol}_{\text{covered site}} \cdot \text{mol}_{\text{total site}}^{-1}$
θ_j = fractional coverage by the species j, $\text{mol}_{\text{species}_j} \cdot \text{mol}_{\text{total site}}^{-1}$
θ_r = assumed coverage of species j, $\text{mol}_{\text{species}} \cdot \text{kg}_{\text{sorbent}}^{-1}$
θ_f = solid tracer concentration in the inlet regenerated sorbent stream, $\text{mol}_{\text{species}} \cdot \text{kg}_{\text{sorbent}}^{-1}$
ρ_s = sorbent particle density, $\text{kg}_{\text{sorbent}} \cdot \text{m}_{\text{particle}}^{-3}$
ρ_g = density of the gas, $\text{kg} \cdot \text{m}^{-3}$
μ = viscosity of the gas, $\text{kg} \cdot \text{m}^{-1} \cdot \text{s}^{-1}$
ϵ_g = void fraction of the riser, $\text{m}_{\text{gas}}^3 \cdot \text{m}_{\text{reactor}}^{-3}$
τ_g = mean residence time of the gas phase, s
τ_s = mean residence time of the sorbent, s
β = interphase momentum transfer coefficient, $\text{kg} \cdot \text{m}^{-3} \cdot \text{s}^{-1}$
β = number of sites covered by the complex surface species, $\text{mol}_{\text{site}} \cdot \text{mol}_{\text{species}}^{-1}$ (Tables 2 and 3)

Subscripts

g = fluid
s = solid
t = terminal
w = tube wall
rg = regenerated sorbent
rc = recycle sorbent

Literature Cited

Bi, H. T., and L. S. Fan, "Regime Transitions in Gas-Solid Circulating Fluidized Beds," AIChE Meeting, Los Angeles (1991).

Brereton, C. M. H., J. R. Grace, and J. Yu, "Axial Gas Mixing in a Circulating Fluidized Bed," *Circulating Fluidized Bed Technology II*, Pergamon, Toronto, p. 307 (1992).

De Wilde, J., A. K. Das, G. H. Heynderickx, and G. B. Marin, "Development of a Transient Kinetic Model for the Simultaneous Adsorption of SO_2-NO_x over Na/γ-Al_2O_3 Sorbent," *Ind. Eng. Chem. Res.*, **40**, 119 (2001).

De Wilde, J., and G. B. Marin, "Investigation of Simultaneous Adsorption of SO_2 and NO_x on Na/γ-Al_2O_3 with Transient Techniques, *Catal. Today*, **62/4**, 321 (2000).

Fei, W., R. Xing, Z. Rujin, L. Guohua, and J. Yong, "A Dispersion Model for Fluid Catalytic Cracking Riser and Downer Reactors, *Ind. Eng. Chem. Res.*, **36**, 5049 (1997).

Felsvang, K., V. Boscak, S. B. Iversen, and P. Andersen, "Update on SNAP Technology for Simultaneous SOx and NOx Removal; EPRI-DOE- EPA Combined Utility Air Pollutant Control Symposium, The Mega Symposium, Atlanta, GA (1999).

Fu, B., H. Weinstein, B. Brenstein, and A. B. Shaffer, "Residence Time Distribution of Recycle Systems. Integral Equation Formulation," *Ind. Eng. Proc. Des. Dev.*, **10**, 501 (1971).

Gear, C. W., *Numerical Initial Value Problems in Ordinary Differential Equations*, Prentice-Hall, Englewood Cliffs, NJ, p. 37 (1971).

Gidaspow, D., *Multiphase Flow and Fluidization, Continuum and Kinetic Theory Descriptions*, Academic Press, San Diego, p. 34 (1994).

Godfroy, L., G. S. Patience, and J. Chaouki, "Radial Hydrodynamics in Risers, *Ind. Eng. Chem. Res.*, **38**, 81 (1999).

Graf, R., "First Operating Experience with a Dry Flue Gas Desulfurization (FGD) Process Using a Circulating Fluid Bed (FGD–CFB)," *Circulating Fluidized Bed Technology: First Conference Proceedings*, Pergamon Press, Halifax, N. S., Canada, p. 317 (1985).

Hydrocarbon Processing, "Summary on Environmental Processes '98," 71 (1998).

Jeh, J. T., W. T. Ma, H. W. Pennline, J. L. Haslbeck, J. I. Joubert, and F. N. Gromicko, "Integrated Testing of the NOXSO Process —Simultaneous Removal of SO_2 and NO_x from Flue Gas," *Chem. Eng. Commun.*, **114**, 65 (1992).

Kiel, J. H. A., W. Prins, and W. P. M. Van Swaaij, "Modelling of Non-Catalytic Reactions in a Gas Solid Trickle Flow Reactor: Dry, Regenerative Flue Gas Desulfurization Using a Silica Supported Copper Oxide Sorbent," *Chem. Eng. Sci.*, **47**, 4271 (1992).

Lapidus, L., *Digital Computation for Chemical Engineers*, McGraw-Hill, New York, p. 286 (1962).

Lin, W., and C. M. van den Bleek, "The SO_x–NO_x Emission in the Circulating Fluidized Bed Combustion of Coal," *Circulating Fluidized Bed Technology: Third Conf. Proc.*, Japan, p. 6-2-1 (1990).

Mok, Y. S., and S. W. Ham, "Conversion of NO to NO_2 in Air by a Pulsed Corona Discharge Process," *Chem. Eng. Sci.*, **53**, 1667 (1998).

Nieuwland, J. J., M. V. S. Annaland, J. A. M. Kuipers, and W. P. M. van Swaaij, "Hydrodynamic Modeling of Gas Particle Flows in Riser Reactors," *AIChE J.,* **42**, 1569 (1996).

Nieuwland, J. J., E. Delnoij, J. A. M. Kuipers, and W. P. M. van Swaaij, "An Engineering Model for Dilute Riser Flow," *Powder Technol.*, **90**, 115 (1997).

Patience, G. S., and J. Chaouki, "Gas Phase Hydrodynamics in the Riser of a Circulating Fluidized Bed," *Chem. Eng. Sci.*, **48**, 3195 (1993).

Pita, J. A., and S. Sundaresan, "Developing Flow of a Gas-Particle Mixture in a Vertical Riser," *AIChE J.*, **39**, 541 (1993).

Pugsley, T. S., G. S. Patience, F. Berruti, and J. Chaouki, "Modeling the Catalytic Oxidation of n-Butane to Maleic Anhydride in a Circulating Fluidized Bed Reactor," *Ind. Eng. Chem. Res.*, **31**, 2652 (1992).

Rhodes, M., *Introduction to Particle Technology*, Wiley, Chichester, p. 142 (1998).

Theologos, K. N., and N. C. Markatos, "Advanced Modeling of Fluid Catalytic Cracking Riser-Type Reactors," *AIChE J.*, **39**, 1007 (1993).

Wong, R., T. Pugsley, and F. Berruti, "Modeling the Axial Voidage Profile and Flow Structure in Risers of Circulating Fluidized Beds," *Chem. Eng. Sci.*, **47**, 2301 (1992).

Appendix: Residence Time Distribution in a Riser with Solid Recycle

RTD based on the response to a tracer step function

Let θ_f be the concentration in $\text{mol}_{\text{species}} \cdot \text{kg}_{\text{sorbent}}^{-1}$ of the solid tracer injected into the regenerated sorbent stream of the riser at time $t = 0$ (Figure 1). The residence time distribution (RTD) of the solid inside the riser is obtained by monitoring the concentration of the tracer in the spent sorbent stream. The single-pass solid residence time τ_{s1} in the riser with a fully developed flow and negligible slip is given by

$$\tau_{s1} = \frac{V_r}{Au_s} = \frac{V_r}{A(u_g - u_t)} \approx \tau_g = \frac{V_r}{F_g}. \tag{A1}$$

As is evident from Eq. A1, τ_{s1} depends primarily on the gas volumetric flow rate and not on the solid flow rates.

The incremental change in the tracer concentration in the outlet (spent sorbent stream) after a single pass is expressed as

$$\Delta\theta_1 = \frac{\theta_f}{(R+1)}, \tag{A2}$$

where

$$R = \text{Recycle ratio of the solid} = \frac{G_{s,rc}}{G_{s,rg}}. \tag{A3}$$

The incremental change in the outlet tracer concentration after the ith pass as obtained by Fu et al. (1971) is

$$\Delta\theta_i = \theta_i - \theta_{i-1} = \frac{\theta_f}{(R+1)}\left(\frac{R}{R+1}\right)^{i-1} = \Delta\theta_1\left(\frac{R}{R+1}\right)^{i-1}. \tag{A4}$$

The sum of all the incremental changes over infinite passes S is given by

$$S = \sum_{i=1}^{\infty} \Delta\theta_i = \frac{\theta_f}{(R+1)}(R+1) = \theta_f, \tag{A5}$$

which is equal to the magnitude of the step input.

Hence, the residence time distribution of the solid in the riser E_i, defined as the fractional incremental change in the species coverage between the $i-1$ and the ith pass following the tracer step function, is given by

$$E_i = \frac{\Delta\theta_i}{S} = \frac{1}{R+1}\left(\frac{R}{R+1}\right)^{i-1}. \tag{A6}$$

RTD from the convergence error in the recycle loop

Let θ_r be the assumed coverage in $\mathrm{mol_{species}} \cdot \mathrm{kg^{-1}_{sorbent}}$ in the total recycle sorbent stream of a species, j. From Eq. 8, assuming the regenerated sorbent has no species, the coverage of species j in the sorbent mixture at the riser inlet is

$$\theta_{i1} = \theta_r\left(\frac{R}{R+1}\right). \tag{A7}$$

The coverage of species j at the end of the riser after a single pass, that is, after the first iteration is given by

$$\theta_{o1} = \theta_{i1} + f_1, \tag{A8}$$

where f_1 is the change in the same species coverage due to the reactions in the riser.

The convergence error $\Delta\theta_i$ is defined as the difference between the species coverage at the outlet after the $i-1$th iteration and the ith iteration. After the first iteration, the convergence error is

$$\Delta\theta_1 = \theta_r - \theta_{o1} = \frac{\theta_r}{R+1} - f_1. \tag{A9}$$

The incremental change in the convergence error after the ith iteration is expressed as

$$\Delta\theta_i = \frac{\theta}{R+1}\left(\frac{R}{R+1}\right)^{i-1} + \frac{f_1}{R+1}\left(\frac{R}{R+1}\right)^{i-2} + \frac{f_2}{R+1}\left(\frac{R}{R+1}\right)^{i-3} + \cdots - f_i. \tag{A10}$$

Assuming that the variation in the change-of-species coverage due to the reactions in different iterations is negligible,

$$f_1 = f_2 = \cdots = f_i. \tag{A11}$$

Then Eq. A10 can be simplified as

$$\Delta\theta_i = \left(\frac{R}{R+1}\right)^{i-1}\left[\frac{\theta_r}{R+1} - f_1\right] = \Delta\theta_1\left(\frac{R}{R+1}\right)^{i-1}. \tag{A12}$$

The sum of all errors S after many iterations can be expressed as

$$S = \sum_{i=1}^{\infty} \Delta\theta_i = \Delta\theta_1(R+1) = \theta_r - (R+1) f_1. \tag{A13}$$

Equation A13 provides the magnitude of the step change in the case of the RTD study, based on the convergence error in the recycle loop.

Hence the fractional incremental change in the species coverage between the $i-1$ and ith iterations is given by

$$E_i = \frac{\Delta\theta_i}{S} = \frac{1}{R+1}\left(\frac{R}{R+1}\right)^{i-1}. \tag{A14}$$

It is seen that Eqs. A6 and A14 are identical.

Manuscript received Dec. 15, 2000, and revision received May 24, 2001.